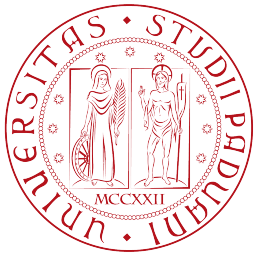

UNIVERSITÀ DEGLI STUDI DI PADOVA

Dipartimento di Fisica e Astronomia "Galileo Galilei"

Bachelor Degree in Physics

Final Dissertation

Characterization of highly-segmented silicon detectors for direct reactions with radioactive beams

Thesis supervisor

Prof. Daniele Mengoni

Thesis co-supervisor

Dr. Alain Goasduff

Candidate

Riccardo Lombardi

Academic Year 2019/2020

Abstract

The aim of this work was to characterize two large-area, highly-segmented, 1.5-mm thick silicon detector prototypes, with the goal of using them during in-beam experiments, in order to investigate nuclear structure properties by particle and gamma-ray spectroscopy.

Such characterization consisted, after having identified the depletion voltage by different approaches, in the estimate of the best energy and time resolution. In the case of the energy resolution, optimal filter parameters have been determined by a scan and by applying the FFT transform to identify the main noise contributions. Timing properties have been scrutinized using a digital constant-fraction algorithm to efficiently restrain time jitter and walk. Eventually an estimate of charge-sharing effects and resistivity of the substrate have been achieved.

Contents

Abstract **3**

1 Introduction **7**

2 Experimental Setup **9**
2.1 Semiconductior Detector: Silicon Diode 9
2.2 Test Bench and Read-out Chain 9

3 Data Analysis **11**
3.1 Depletion Voltage 11
3.2 Energy Resolution 14
3.2.1 FFT and Parseval Theorem 16
3.3 Timing 19
3.4 Charge-Sharing signals 21
3.5 Resistivity 22

4 Conclusions and Perspectives **25**

5 Bibliography **27**

Chapter 1

Introduction

One of the main tool to investigate nuclear properties faraway from the valley of beta stability is to analyze the products of direct reactions or transfer reaction using inverse kinematics with radioactive beams. Such measurements suffer of decreasing cross section moving away from stable nuclei. Direct reactions are typically binary, therefore by measuring energy and angular distribution of one of the reaction products it is possible to reconstruct the excitation energy of the reaction partner. In most cases it is needed to measure at the same time different kind of direct reactions, to reach this goal it is necessary to use a modular set-up covering a large range of angles with a satisfactory position resolution. To overcome the limits of this approach an efficient instrument is necessary, typically array of silicon detectors, at need combined with gamma-ray detectors [1].

The aim of this work is to characterize two thick detector prototypes, elements of the GRIT array, obtained from a FZ ingot and grown on a 6-inch technology. Detectors have been manufactured by Micron Semiconductor Ltd [2]. Junction and ohmic sides are electrically segmented in 128 strips, which are orthogonal each other on both sides of the detectors.

A schematic representation of the detector can be seen in Fig. 1.1. The segmentation of the active surface allows a better angular distribution and the perpendicular strips give information about particle position. Nevertheless these improvements come at a cost, a great number of channels has to be read. Also, the electric charge generated by one event can be read by more than one strip, producing the charge-sharing signals and reducing then the total active area of about 10%. Moreover there are transient signals and cross-talk signals, produced through induction between strips. These effects need to be evaluated because they generate a sistematic error on energetic measurements.

In this work, two 1.5-mm thick detectors will be tested coded TTT-1500, grade A and B. As a reference, data from a 500-μm thick detector, obtained from the same manufacturing technique, are reported at need.

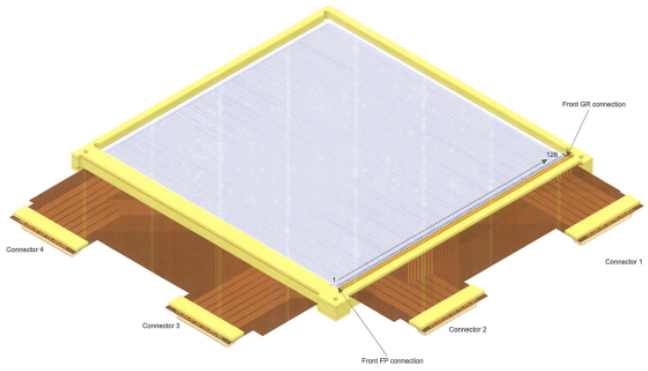

Figure 1.1: A schematic representation of tested detectors. Each side of the junction has 128 strips, connected to the electronics trough four Kapton cables and connectors..

Chapter 2

Experimental Setup

2.1 Semiconductior Detector: Silicon Diode

One of the most common method to obtain a ionizing radiation detector is to get a p-n junction, through heavy doping of a semiconductor crystal, and then reverse bias it, in order to deplete the bulk of free charges. In this way all the charges produced by the incident radiation can be collected.
Nowadays semiconductor detectors are considered a standard in particle spectroscopy for the optimal energy resolution and the capability to be manufactured in different shapes and dimensions [3].

2.2 Test Bench and Read-out Chain

The test bench used for detector characterization is presented in Fig. 2.1. The detector was placed in a vacuum chamber at a pressure of 2×10^{-2} mbar. Detector signals were collected by four preampflifiers, via custom adapter boards. The first two are connected to the p side and polarized with the negative bias voltage used to create the depletion region in the detector, instead the second two were connected to the n side and grounded.
The readout consisted in a commercial CAEN V1730 16 Channels 14 bit 500 MHz digitizer, therefore only 16 channels were read at the same time.
The radioactive source used for tests was a single-peak ^{241}Am, emitting 5.486-MeV α particles.

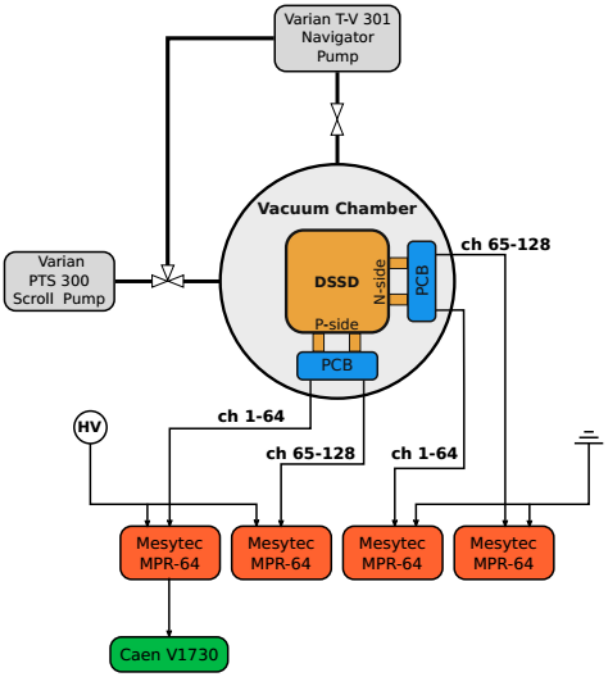

Figure 2.1: In the test bench, the detector is located in a reaction chamber and and signals are sent via four preamplifiers to the digitizer. The p side is bias to depletion voltage, whilst the opposite electrodes on the n side are grounded.

Chapter 3

Data Analysis

3.1 Depletion Voltage

As previously discussed, the bulk of the detector needs to be depleted from the majority charge carriers. Experimentally, the depletion voltage can be mapped by plotting IV curve of the detector, and then it is identified with the presence of a plateau in the IV plot.
As we can see in Fig. 3.1, manufacturer data sheet is not well reproduced by our experimental data for the 1.5-mm grade A detector. The leakage current in a semiconductor detector can be reduced by giving voltage to the guard-ring and filed-plate electrodes, on the junction and ohmic side, respectively, in order to reduce the surface voltage gradients. Despite these improvements, the presented curve didn't change.
Eventually, 60 V was tentatively chosen as working voltage, because at the footing of a change in the slope in the IV curve.
The same test has been performed for the grade B detector, but the leakage current rose to 1 mA after 20 V bias. To avoid damaging the detector with the massive current the test was stopped and the detector was declared malfunctioning.
As a reference here, we also report the IV curve for the 500-μm thick detector. In this case the IV curve is compliant with the manufacturer data sheet.
Qualitatively, we can notice how the thickness of the silicon bulk modifies the leakage current: in the thicker one the current is 3.5 to 5 times greater than in the thinner, which is compliant with the volume ratio of the two detectors.

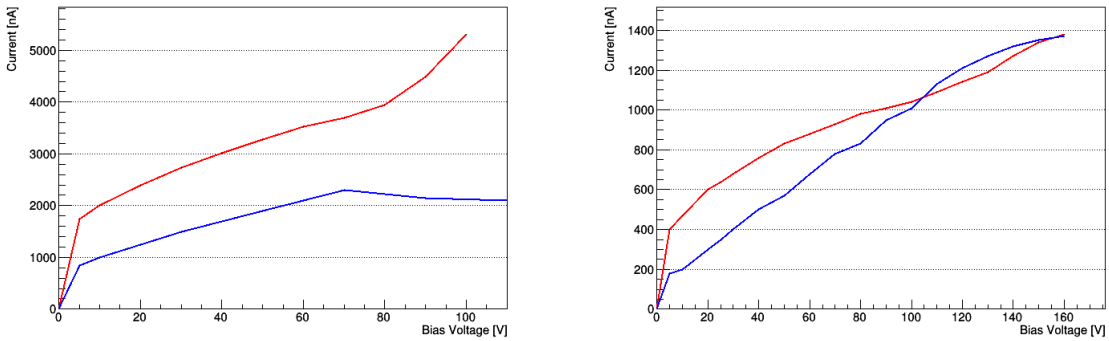

Figure 3.1: Experimental (in red) vs Constructor's (in blue) IV curve for the 1.5-mm grade A (left) and 500-μm (right) detector.

In absence of a clear plateau in the IV plot of the 1.5-mm thick detector, complementary methods were adopted to identify the operation voltage of the silicon prototype: the decrease in rise time and the gain of the energy centroid. Both the method should give a reference value when reaching the depletion voltage. In particular, to optimize the following work, it is useful to have a quick rise in the signals.

As we can see from the left panel of Fig. 3.2, for the 1.5-mm thick detector, until a bias voltage of 70 V, signals have a fairly long rise time; in these conditions some of the charge generated by the radiation could be lost, lowering the height of the signal.
As a reference, the situation is similar to what happens with the 500-μm thick detector, see Fig.3.2, on the right panel.

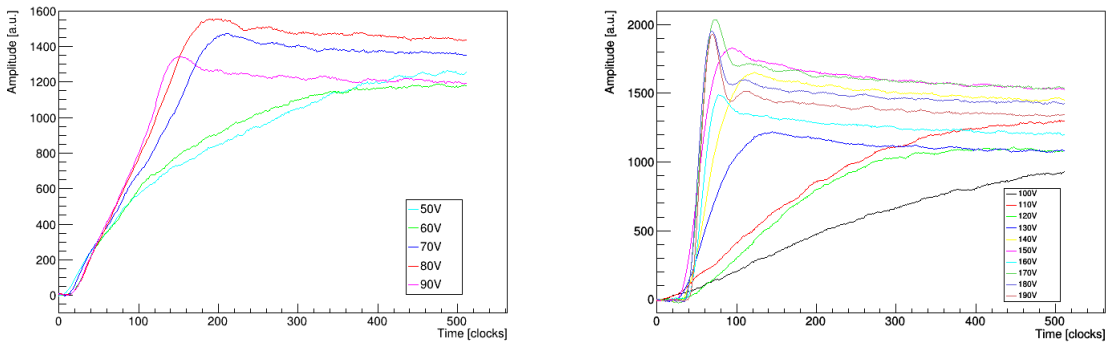

Figure 3.2: Various signals captured at different voltages for the thick and thin detectors, respectively.

A more precise method to find the depletion voltage is based on centroid channel shift as a function of the applied voltage. However, this approach was not possible for the thick detector, due to the large leakage current. Therefore, in the remaining part of the present paragraph we present the result for the 500-μm thick detectors, when the former approach is applied.
In order to estimate the energy shift, preamplifier signals have been processed by using a custom frequency filter. The parameters of such trapezoidal filter were optimized since they depend on structural parameters such as detector thickness and surface but they also depend on variables like the bias and the parasitic capacitance of the junction. The same parameters have been kept constant during the measurements.
As can be seen in Fig. 3.3, a steep change in the slope starts at about 140 V voltage, therefore we conclude that such value corresponds to the depletion voltage for the 500-μm thick detector.
The result of the different approaches can be seen in Table 3.1. As mentioned above the 1.5-mm grade B detector is unusable due to the high leakage current. In all the subsequent analysis, depletion voltage is assume to be 70 and 130 V for the 1.5-mm thick and 500-μm thick detector, respectively.

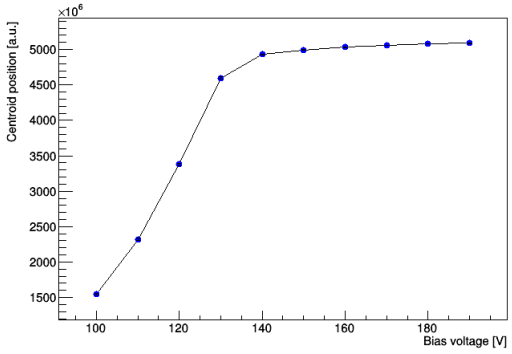

Figure 3.3: Position of the peak, due to the ^{241}Am source decay, as function of the bias for the thin detector.

	500-μm	1.5-mm grade A	1.5-mm grade B
IV curve	100 V	60 V	-
Rising time	130 V	70 V	-
Energy peak	130 V	-	-

Table 3.1: Different results of the depletion voltage for each detector depending on the applied method.

3.2 Energy Resolution

Energy of the impinging radiation can be derived from the maximum of the preamplifier signal. In our case a trapezoidal filter has been used. It is a recursive algorithm that converts the pulse $v(n)$ form the preamplifier to a symmetrical trapezoidal pulse $s(n)$ given by

- $d^{k,l}(n) = v(n) - v(n-l) - v(n-k) + v(n-k-l)$
- $p(n) = p(n-1) + d^{k,l}(n)$
- $r(n) = p(n) + Md^{k,l}(n)$
- $s(n) = s(n-1) + r(n)$

where $v(n)$, $p(n)$ and $s(n)$ are equal to zero if $n < 0$ and $M = 1/(exp(T_{clk}/\tau) - 1)$ depends on the digitizer clock and signal decay time [4]. An example of filter application is shown in Fig. 3.4. In addiction, the parameters l and k need to be optimized to make the trapezoid flat top as flat as possible: using this filter the information about particle energy is carried by the height of the flat top with respect to the base line.

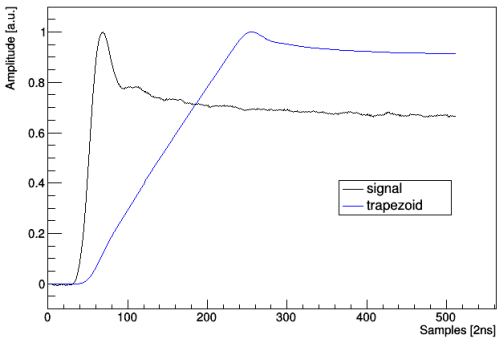

Figure 3.4: Example of trapezoidal filter, both signal and the trapezoid has been rescaled to their maximum,

To achieve the optimal parameters I wrote an algorithm which computes the resolution $R = FWHM/H_0$ of the peak for each (k, l) couple in a defined range, results are shown in Fig. 3.5.
For the 1.5-mm grade A detector the best parameters for the p side are $k = 2700$, $l = 440$ with a resolution $R = (3.18 \pm 0.08)\%$, whereas for the n side $k = 2600$, $l = 380$ and $R = (3.41 \pm 0.09)\%$. The parameters are slightly different but the most important thing is that, as we can see from Fig. 3.6, the α particles coming from the source located in front of the p side don't penetrate enough in the detector to generate the same amount of events on the n side. This effect is completely absent in the 500 μm detector, so it is probably due to the quality of the detector.

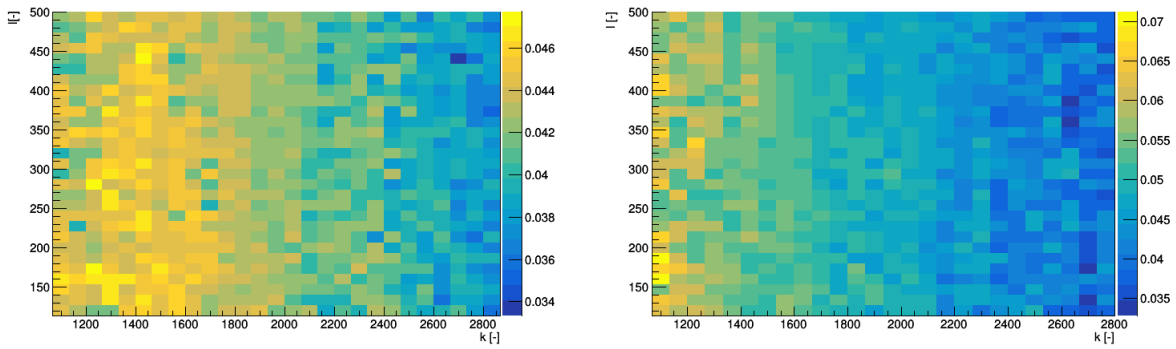

Figure 3.5: Optimization matrices for p (left) and n side (right) of the thick detector, it is shown the resolution of the energy peak as function of the trapezoid parameters, k and l.

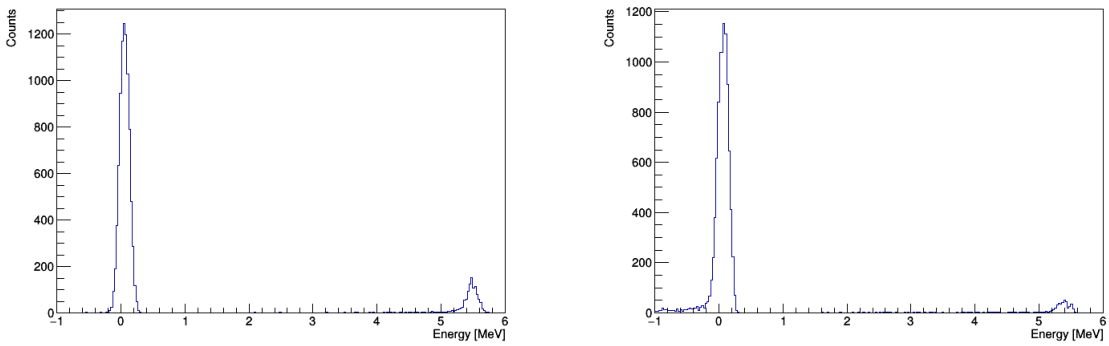

Figure 3.6: Energy frequency for p and n side, thick detector.

A parameter optimization, similar to the above, was performed for the 500-μm thick detector, results are shown in Fig. 3.7. In this case the optimal parameters for energy resolution are $k = 2900$, $l = 370$ on the p side, whereas on the n side the optimizations read $k = 2700$, $l = 350$. The sets of values are comparable for the two sides, as expected.

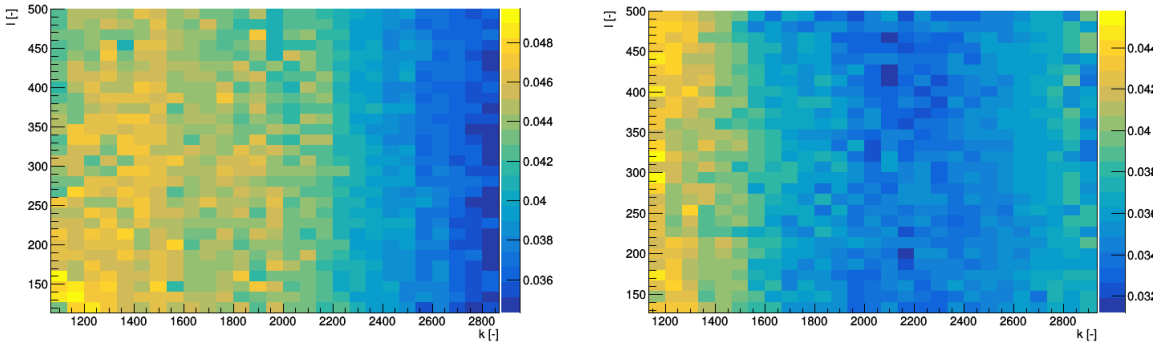

Figure 3.7: Optimization matrix for p and n side of the thin detector, it is shown the resolution of the energy peak as function of the trapezoid parameters, k and l

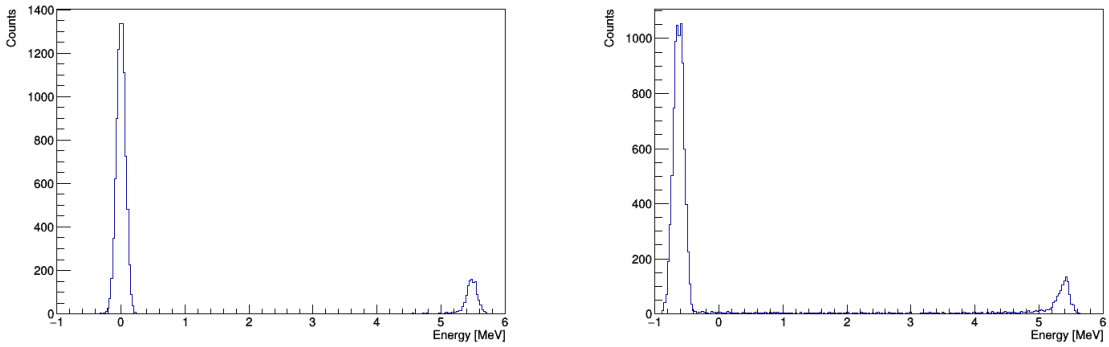

Figure 3.8: Energy frequency for p and n side, thin detector.

	1.5-mm grade A		500-μm	
	p side	n side	p side	n side
k, l	2700, 440	2600, 380	2900, 370	2700, 350
resolution [%]	3.18±0.08	3.41±0.09	3.12±0.03	3.31±0.02

Table 3.2: Final values for the optimal parameters and the energy resolution of each detector.

3.2.1 FFT and Parseval Theorem

In order to check the impact of the electronics noise the Fast Fourier Transform (FFT) was computed. The algorithm was applied to signals with and without radioactive source, in fact, the presence the source covers the noise effect in relative low-frequency domain. The coefficients of the FFT are defined as

$$X_k(f) = \sum_{n=0}^{N-1} x_n(t) e^{-2\pi i k n/N} \qquad k = 0, ..., N-1$$

where N is the number of samples of each trace, $X(f)$ is the complex Fourier transform in the frequency domain and $x(t)$ is the signal in the time domain. Each signal has been renormalized to its maximum, and then the FFT was computed, results are shown in Fig. 3.9 and Fig. 3.10.

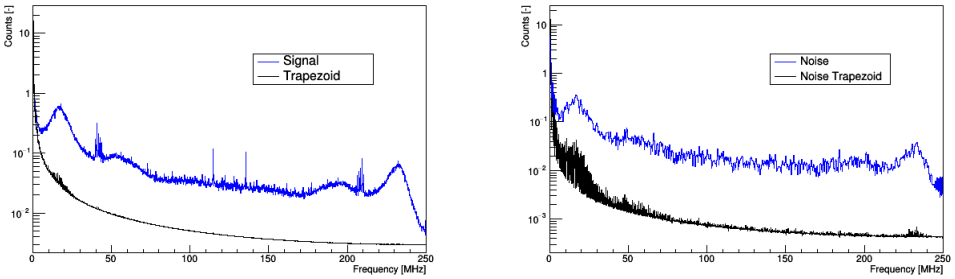

Figure 3.9: Average FFT of signals and noise before and after trapezoidal filter, 1.5-mm grade A detector.

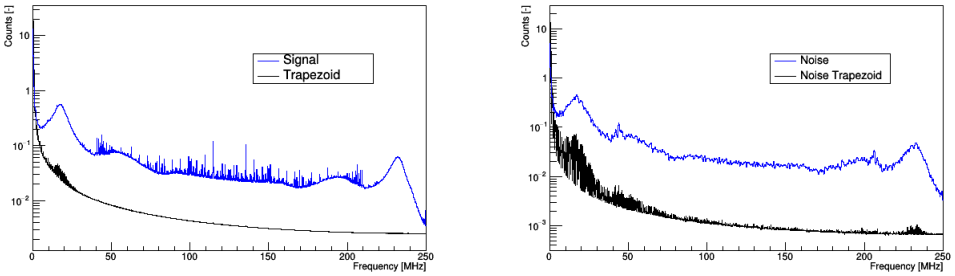

Figure 3.10: Average FFT of signals and noise before and after trapezoidal filter, 500-μm detector.

Trapezoidal filter parameters can be chosen to minimize the noise, whose power is represented in the FFT spectrum. In order to estimate the noise contribution as a function of the effective shaping time, which is linked to the filter parameters, the following theorem is essential:

Parseval's Theorem. *Let $g(t)$ have Fourier Transform $G(f)$. Then the following equation is true*

$$\int_{-\infty}^{\infty} |g(t)|^2 dt = \int_{-\infty}^{\infty} |G(f)|^2 df$$

The theorem is valid also for Discrete Fourier Transform (DFT):

Parseval's Theorem for discrete functions. *Given a discrete function $x_n(t)$ and its DFT $X_k(f)$ defined as*

$$x_n(t) = \frac{1}{\sqrt{N}} \sum_{k=0}^{N-1} X_k(f) e^{2\pi i k n/N} \qquad n = 0, ..., N-1$$

$$X_k(f) = \sum_{n=0}^{N-1} x_n(t) e^{-2\pi i k n/N} \qquad k = 0, ..., N-1$$

the following equation is verified

$$\sum_{n=0}^{N-1} |x_n|^2 = \frac{1}{N} \sum_{n=0}^{N-1} |X_n|^2$$

In our case if $x_n(t)$ is the voltage coming from the preamplifiers then its square magnitude is proportional to the energy of the signal. Parseval's Theorem states that in the FT, equivalently in the DFT, the amount of energy is exactly the same.

Directly from the Parseval's Theorem, in case of a discrete function, we can derive

$$\frac{1}{N} \sum_{n=0}^{N-1} |x_n|^2 = \frac{1}{N^2} \sum_{n=0}^{N-1} |X_n|^2 \implies \sigma^2 = \frac{1}{N^2} \sum_{n=0}^{N-1} |X_n|^2 = \frac{2 \cdot INP}{N^2}$$

$$FWHM = \sigma \sqrt{8ln(2)} \approxeq 3.33 \cdot \sqrt{\frac{INP}{N^2}}$$

The signals were filtered with the trapezoid and then the FFT was computed. In Fig. 3.11 we can see the integral of the FFT, equivalent to the FWMH of the noise as function of the parameters.

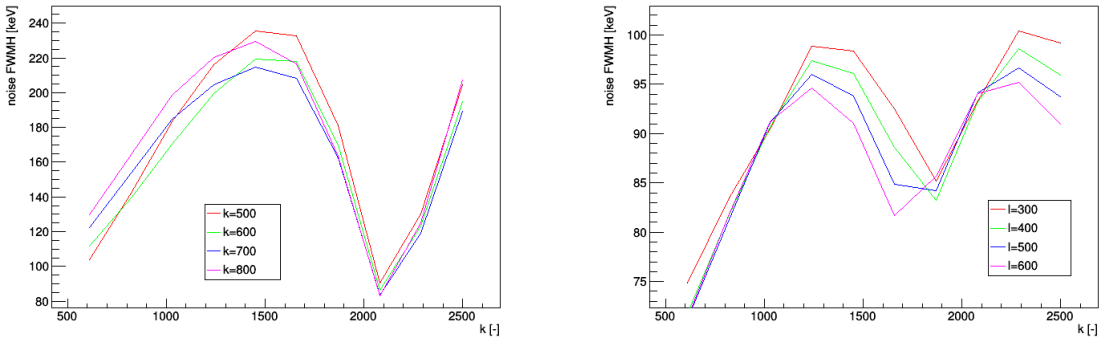

Figure 3.11: Mean value of the noise as function of the trapezoid's parameters, thick and thin detector.

We can appreciate that in both cases the functions have a minimum, corresponding to the parameters which reduces better the noise frequency. Given the definition of shaping time of a signal as the full width of the pulse at half its maximum value, we can express the parameters couple trough the shaping time. For the 1.5-mm grade A detector the appropriate shaping time in order to reduce the noise is 4.6 μs while for the thin detector is 4.2 μs.

The existence of a minimum in the noise as function of the shaping time is expected by the fact that the total noise is the sum of three main contribution: the first one is in series, the second in parallel and the latter is the Flicker noise. While the Flicker noise intensity is inversely proportional to the frequency, the contribution of series noise becomes more important with a smaller shaping time and the parallel noise has the reverse behavior. The trend of the different contributions is shown in Fig. 3.12.

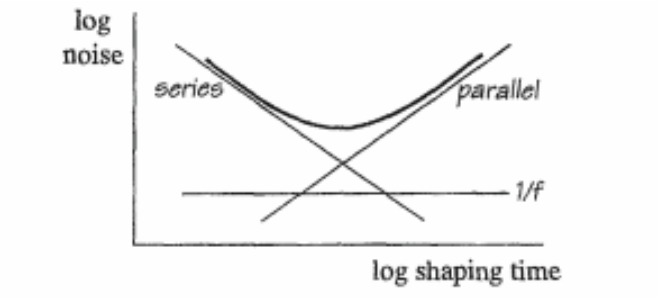

Figure 3.12: Contribution of the three types of noises as functions of the shaping time [3].

3.3 Timing

Time resolution is a parameter of paramount importance in the characterization of a particle detector. In fact, as a particle is detected, a time reference is needed to reconstruct an event and extract other observables, as for example the time of flight. There are two different factors which reduce the resolution: electrical noise, that produces the time jitter, and the different height of each signal, that causes the time walk [3].
There are two main algorithms to extract the time information. One of the most efficient against time jitter and time walk is the Constant Fraction Discriminator (CFD). It is based on three steps:

- The original signal is delayed by a t_d
- The same signal is attenuated by a factor A
- The two signals are added together

The bipolar signal obtained by the CFD algorithm has a zero crossover regardless of the height of the original signal [5]. An example of the CFD is shown in Fig. 3.13.

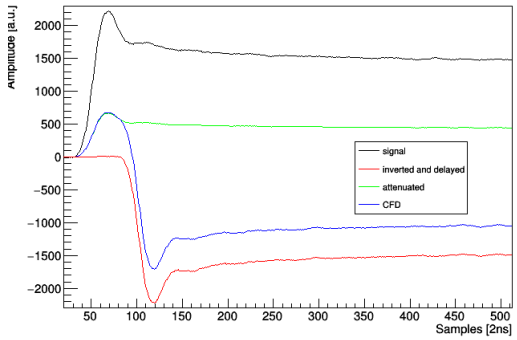

Figure 3.13: Application of the CFD algorithm.

To estimate the optimal resolution a parameter scan was necessary. As in the case of the trapezoidal filter, we wrote an algorithm which built the graph of time difference for each (A, t_d) couple, and then fitted it with a gaussian function.
The result for p side of the 1.5-mm thick grade A detector is shown in Fig. 3.14. The best parameters in this case are $A = 0.25$, $t_d = 30$ which leads to a resolution of (3.02 ± 0.16) ns. Unfortunately, because of the poor statistic, on the n side the optimization was not possible.

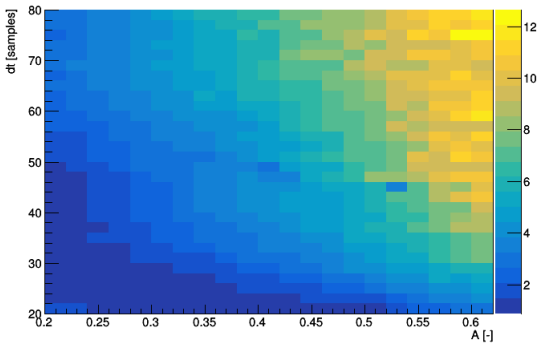

Figure 3.14: CFD optimization for p side, it is shown the time resolution as function of the parameters of the CFD, t_d and A.

For the 500-μm detector it was also possible the optimization of the n side since, as discussed in the previous section, at depletion voltage, signals were generated on both sides of the detectors. In Fig. 3.15 we can observe that the optimal parameters for the CFD algorithm are $A = 0.58$, $t_d = 25$ on the

p side, whereas on the n side the optimization returns $A = 0.48$, $t_d = 25$.
As expected, the time resolution is heavily affected by the working condition of the detector. In the condition of the 1.5-mm thick detector, which is not fully depleted, the charges produced by the radiation slowly drift to anode and cathode, therefore the signal rise time is slow and harder to trigger.

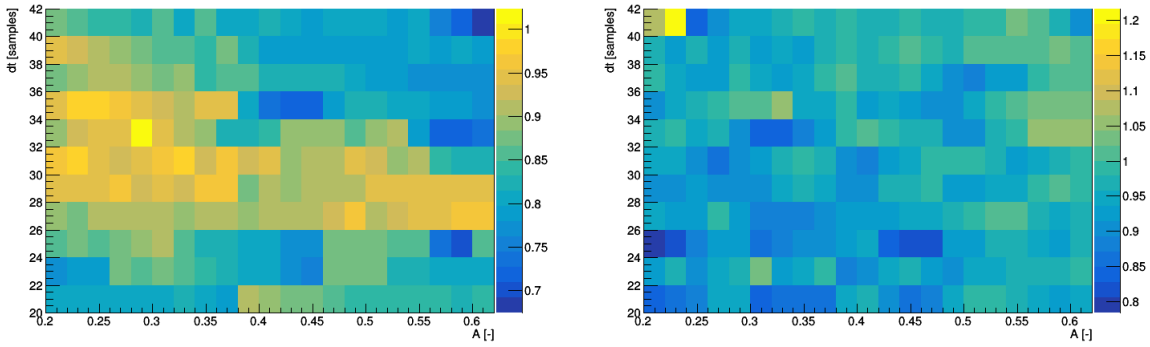

Figure 3.15: CFD optimization matrices for p and n side of the thin detector.

	1.5-mm grade A		500-μm	
	p side	n side	p side	n side
A, t_d	0.25, 30	-	0.60, 25	0.45, 25
resolution [ns]	3.02±0.16	-	1.5±0.05	1.20±0.09

Table 3.3: Summary values for the optimal parameters and the energy resolutions of each detector.

3.4 Charge-Sharing signals

Due to the interaction position of the incident particles, the generated charge could be shared among contiguous strips. The distribution of the time difference as function of the energy deposited on each strip can be also used to obtain the time resolution.
The first step is to isolate the charge-sharing events between two contiguous strip: these events are in the diagonal of the energy correlation matrix between the strips, as shown in the left panels of Fig. 3.16 and Fig. 3.17.
Then, for each point the difference between the CFD zero crossing time of the relative signals were computed and plotted as function of the energy, Fig. 3.16 and Fig. 3.17, right panels. This was possible because the digitizer was set in common OR trigger.
The last step is to project the latter graphics in the y-axis and fit the resulting distribution with a gaussian function.
In both the detectors only the analysis on the p side was possible since the radioactive source was placed in front of it.
For the thick detector the resolution is (3.3 ± 0.9) ns, which is compatible with the value found using the CFD with a compatibility ratio of $\lambda = 0.3$.
The analysis for the thin detector returns (1.3 ± 0.7) ns, which is compatible with the previous value with a compatibility $\lambda = 0.04$.

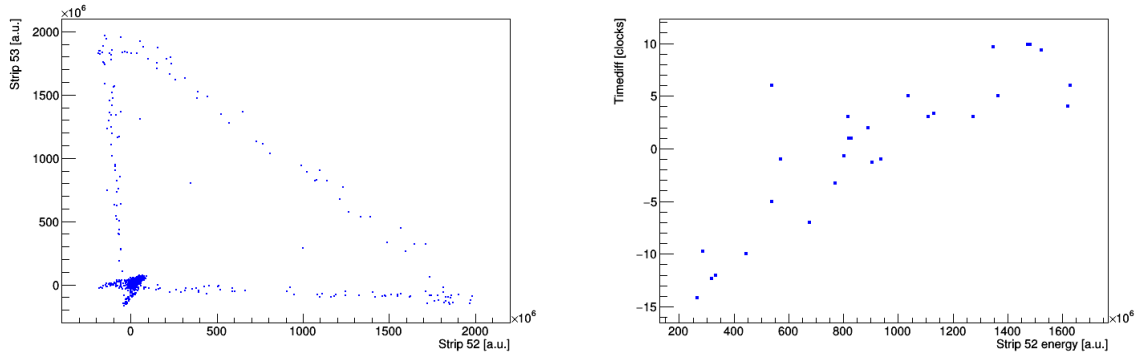

Figure 3.16: Energy correlation matrix for sample strips and difference between trigger times, thick detector.

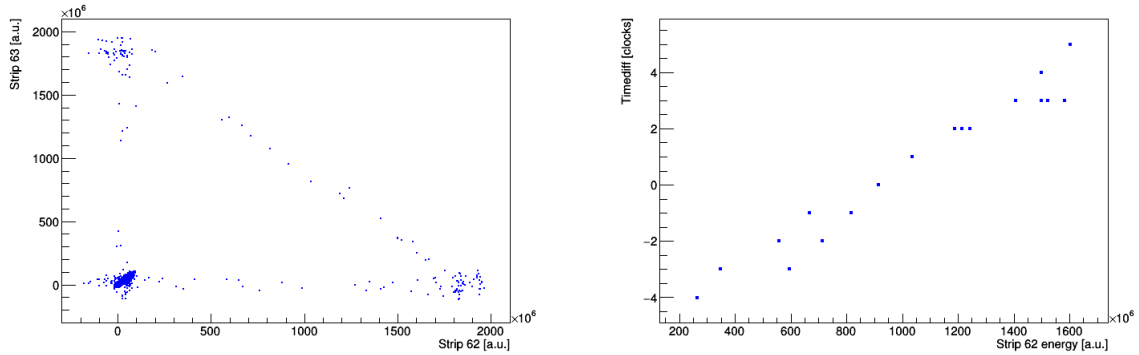

Figure 3.17: Energy correlation matrix for sample strips and difference between trigger times, thin detector.

		1.5-mm grade A	500-μm
Time resolution [ns]	cross-talk	3.3 ± 0.9	1.3 ± 0.7
	CFD	3.02±0.16	1.50±0.05
Compatibility	λ	0.3	0.4

Table 3.4: Summary values of the new estimations of the time resolution compared with the previous ones.

3.5 Resistivity

As proven before, the bias voltage applied to the detector plays a fundamental role in both time and energy resolution. Since the detector is grown from a single silicon crystal and then it is cut, it is likely that some proprieties of the material, such as the resistivity, will not be uniform neither on the thickness nor on the surface of the detector. This means that two particles with the same energy may produce two different signals depending on the point of the detector where they interact.
To have an idea of this effect, it is possible to estimate the resistivity on the detector bulk. Unfortunately, due to the lack of an optimal bias voltage for the thick detector, this test has been made for the 500-μm detector only.
Due to the semiconductor proprieties, in a planar configuration and constant resistivity across the detector thickness, the resistivity is given by:

$$\rho = \frac{d^2}{2V_{dep}\epsilon_g\mu}$$

where d is the detector thickness, $\epsilon_g = 11.7$ is the silicon dielectric constant, μ is the majority-carrier mobility in the detector. Thanks to the orthogonality of the strips, once measured the V_{dep} for each couple of strips, the map of the resistivity can be computed for the whole detector [6].

In analogy to what has been done in the previous part, we know that when the detector is completely depleted, the rise time of the signal is the shortest possible. So one way to get the local V_{dep} for each point is to do a scan of the rise-time of the signal as function of the applied bias, and then fit the data with the following function:

$$t_{rise}(V_{app}) = \begin{cases} t_0 + a(\sqrt{V_{dep}(x,y)} - \sqrt{V_{app}})^2 & \text{for } V_{app} < V_{dep}(x,y) \\ t_0 & \text{for } V_{app} > V_{dep}(x,y) \end{cases}$$

where t_0 is the asymptotic rise-time, when the detector is fully depleted, and a is a coefficient which controls the behavior when the detector is not properly depleted. An example of the process is shown in Fig. 3.18.

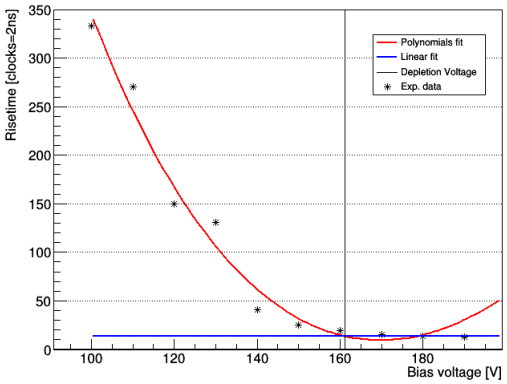

Figure 3.18: Signal rise-time as function of applied bias, fit in linear and non-linear sections, the resulting $V_{dep}(x,y)$ is the intersection between the fits

A square of the first 24 strips was made, in which the mean resistivity is (5.5 ± 0.3) kΩ·cm. However, a full scan is planned in the future. From the Fig. 3.19 we can notice a sort of radial pattern, which we can expect since, as already discussed, the detector is grown from a cylindrical core. Despite this, a mapping on the whole detector would be necessary.

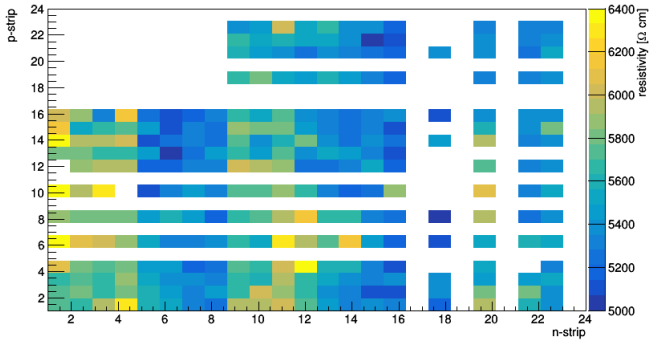

Figure 3.19: Local resistivity on the n side of the detector as function of the numbers of the strips, a blank indicates that the strip is not functioning or there were not enough data to do the fits

Chapter 4

Conclusions and Perspectives

The purpose of this thesis was to characterize two large area, highly-segmented, 1.5-mm thick detector prototypes. Such prototypes are expected to be used during experiments with radioactive beams for particle spectroscopy. However, after a systematic characterization, we concluded that their performances do not suffice for the use during in-beam experiments.

The first part of the work is dedicated to identify the depletion voltage, necessary to operate the detector. For both the 1.5-mm grade A and grade B detectors it was not possible to reach the appropriate depletion voltage due to the high leakage current. Nevertheless the 1.5-mm grade A detector were almost depleted at 70 V, while the grade B detector has been declared non-functional. As a reference, the 500-μm thick detector has a higher depletion voltage, around 140 V, and a lower leakage current of 1.2 μA. We can deduce that the current flowing in the detector is somehow proportional to the thickness of the detector but, since the 1.5-mm grade A and the grade B have the same thickness, the current must also depend on the quality of the detector.

In order to obtain the energy of the impinging radiation a trapezoidal filter was used. Filter parameters has been optimized to get the best energy resolution. For the 1.5-mm grade A the resolution is (3.18$\pm$0.08)% for the p side and (3.41$\pm$0.09)% for the n side. These values are similar to those obtained from the thin detector, which are (3.12$\pm$0.03)% for the p side and (3.31$\pm$0.02)% for the n side.

The FFT transform allowed to describe both the source and noise signals in the frequency domain. The noise contribution was estimated and reduced by applying a trapezoidal filter. The shaping time, which minimizes the noise, was found to be 4.6 μs and 4.2 μs for the 1.5-mm grade A detector and 500-μm detector, respectively. The corresponding noise is $\sim$90 keV for both the detectors.

The timing resolution has also been evaluated, optimizing the CFD parameters. For the 1.5-mm grade A detector only the analysis on the p side were possible due to the partial depletion of the bulk. The best resolution is (3.02 ± 0.16) ns while for the 500-μm thick detector the resolution is (1.5 ± 0.05) ns. Unlike the energy resolution, the timing is heavily afflicted by the uncompleted depletion of the detector. The timing resolution was also estimated using charge-sharing signals. The results are in good agreement with the former ones.

The resistivity was estimated to be (5.5 ± 0.3) kΩ·cm on a limited part of the 500-μm thick detector. As expected the resistivity seems to have a radial symmetry but due to many broken strips and to the small surface tested, a more systematic test has to be performed.

Chapter 5

Bibliography

[1] M. Assié, et al., Nucl. Inst. and Meth. A, 908 (2018) 250-255.

[2] http://www.micronsemiconductor.co.uk/

[3] G.F. Knoll, Radiation Detection and Measurement, third ed., Wiley, New York, 1999.

[4] Valentin T. Jordanov, et al., Nucl. Inst. and Meth. A, 353 (1994) 261-264.

[5] N. Cieplicka-Oryńczak, et al., Eur. Phys. J. A (2018) 54: 209.

[6] L. Bardelli, et al., Nucl. Instr. and Meth. A, 602 (2009) 501-505.